

# Study of the cluster formation in low-temperature systems. Spectral manifestation of resonance dipole–dipole interactions between nondipole polyatomic molecules

A.N. Cherevatova, V.N. Bocharov, T.D. Kolomiitsova, D.N. Shchepkin, and K.G. Tokhadze

*Physical Faculty, St. Petersburg State University, Peterhof, St. Petersburg 198504, Russia*

E-mail: K.Tokhadze@molsp.phys.spbu.ru

Received January 5, 2010

Resonance dipole–dipole interactions are shown to strongly manifest themselves in fundamental and overtone band shapes of low-temperature systems, consisting of polar and nonpolar molecules as well with a relatively large first derivatives ( $P' > 0.3$  D) of the dipole moment. The rough model on the basis of the interaction between two non-degenerate, doubly degenerate, and triply degenerate oscillators was developed to study pairs of interacting molecules and clusters in low-temperature condensed systems. The concentration dependences of second- and third-order spectral band moments permitted the number of molecules in clusters to be estimated.

PACS: **78.30.–j** Infrared and Raman spectra;

**33.20.–t** Molecular spectra;

36.40.Mr Spectroscopy and geometrical structure of clusters.

Keywords: spectral moments, dipole–dipole interactions, clusters, low-temperature molecular systems.

## 1. Introduction

Structure and dynamics of complex systems in low-temperature condensed phase attract considerable attention of researchers. Band shapes of molecular aggregates were investigated by using different experimental methods [1–6] and theoretical approaches [7–11]. The purpose of present paper is to propose a way to detect the pairs of interacting molecules («dimers») and clusters in low-temperature systems based on studying the resonance dipole–dipole (RDD) interactions, sometimes also called the TD–TD interactions, i.e., the interactions of transition dipole moments. The molecules with large values of the first derivatives of the dipole moment  $P$  with respect to the normal coordinates are taken as the subjects of investigation.

The RDD interaction in low-temperature molecular systems play a major role in forming the spectral band shapes when the derivative of the dipole moment  $P$  with respect to a dimensionless normal coordinate becomes large enough ( $P' > 0.3$  D). The intense fundamental band and overtone bands for a mode with a large value of  $P'$  in the IR absorption are asymmetrically broadened by RDD interaction in the Raman [12–14] and IR absorption spectra of low-temperature molecular liquids consisting of polar or nonpolar molecules [15–17]. By using the RDD interaction

formalism, band shape simulations were performed for the absorption spectra of several liquids ( $\text{CF}_4$ ,  $\text{SF}_6$ ,  $\text{SiF}_4$ ,  $\text{CF}_3\text{Cl}$  and  $\text{CF}_3\text{Br}$ ) at temperatures close to the melting point [18], and the results obtained are in quantitative agreement with the experimental data.

Other mechanisms, such as the rotational diffusion and translational relaxation, have a little impact on the band shapes at low temperature [1,19,20]. The previous studies demonstrated the dominant effect of the RDD interaction on the formation of the vibrational [21–30] and rotational-vibrational [31–32] spectra of dimers. Note that the absorption spectrum of pairs of molecules can be discrete and continuous [33]. The discrete spectrum is observed in matrices, where orientation of molecules in a pair is fixed. For low-temperature liquids the discrete spectrum emerges only when dimer forming molecules have a large dipole moment derivative with respect to the normal coordinates of triply degenerate modes. In the case of less degenerate vibrations, the continuous spectrum is observed.

## 2. Experimental

### 2.1. Low-temperature liquids

Infrared spectra were recorded with a LOMO IKS-24, Bruker IFS-28 and Bruker IFS 66v spectrometers at a reso-

lution of  $0.3\text{--}2\text{ cm}^{-1}$ , which is satisfactory for the studied bands with the half-width  $\Delta\nu_{1/2} \geq 1\text{ cm}^{-1}$ . The spectra of solutions in liquid Ar, O<sub>2</sub>, N<sub>2</sub>, and Kr were studied at relatively low concentration  $C = (0.01\text{--}3) \cdot 10^{-2}$  mole fraction (mf) in the temperature interval  $T = 80\text{--}180\text{ K}$ , using optical liquid cryostats whose path lengths  $l$  vary from 0.4 mm to 10 cm. The employed cryostats have been described in Ref. 34. To record the absorption spectra of solutions with high concentrations ( $C > 10^{-2}$  mf) and of pure liquids, the cryostats with 0.09 and 0.15 mm path lengths were used.

## 2.2. Matrix isolation studies

IR spectra of SF<sub>6</sub>, SiF<sub>4</sub> and CF<sub>4</sub> in low-temperature Ar, N<sub>2</sub> and Ne matrices were recorded at 11 K (Ar, N<sub>2</sub> matrices) and 4.7 K (Ne matrix) with a resolution of 0.25 and 0.12  $\text{cm}^{-1}$  by means of a Bruker 113v FTIR and Bruker IFS/66S spectrometers. The concentration of SF<sub>6</sub> (SiF<sub>4</sub>, CF<sub>4</sub>)/Ar(N<sub>2</sub>, Ne) varied in a range between 1/100–1/16000. The procedure has been previously described in detail in [26].

## 3. Experimental results and discussion

### 3.1. Comparison of liquid-phase spectra with the cryosolution spectra

The striking manifestation of RDD interaction in the spectral band shapes can be illustrated by comparing liquid-phase spectra with those of cryogenic highly diluted solutions at close temperatures. Figure 1 displays the  $\nu_1 + \nu_3$  band shapes of pure liquids and dilute solutions of nonpolar molecules, SF<sub>6</sub> (a) and SiF<sub>4</sub> (b), where  $\nu_1$  is the frequency of the totally symmetric mode and  $\nu_3$  is that of the strong IR-active vibration. For the molecules of interest to us, the dilute solution spectra, at concentration  $C < 10^{-4}$  mf, have the Lorentzian profiles within three or more half-widths and their characteristics are governed by rotational and vibrational relaxation [20]. At the same time, the absorption bands in the spectra of pure liquids exhibit complex asymmetric profiles extending over  $\approx 60\text{ cm}^{-1}$ . It seems likely that the main mechanism of the band shape formation is the RDD interaction because the dipole moment derivative  $P_3'$  has a high value of 0.55 D for SF<sub>6</sub> and

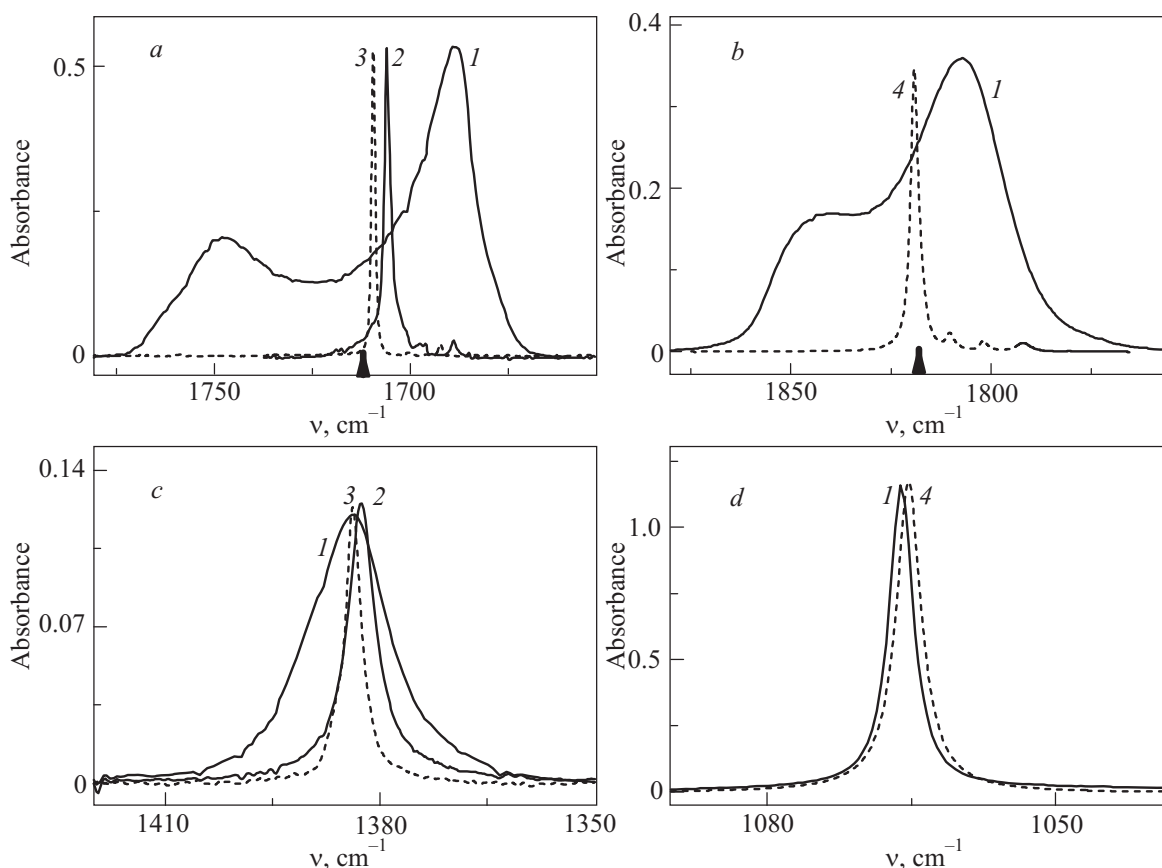


Fig. 1. Infrared spectra of nonpolar molecules in pure liquid phase (1) and dissolved in liquid noble gases (2, 3, 4) at similar temperatures. The  $\nu_1 + \nu_3$  bands of SF<sub>6</sub>, liquid at 222 K with path length  $l = 0.09\text{ mm}$  (1); the solution in liquid Kr at 174 K,  $l = 2\text{ cm}$ ,  $C = 10^{-4}$  mf (2); the solution in liquid N<sub>2</sub> at 83 K,  $l = 2\text{ cm}$ ,  $C = 10^{-4}$  mf (3) (a). The  $\nu_1 + \nu_3$  bands of SiF<sub>4</sub>; liquid at 186 K,  $l = 0.09\text{ mm}$  (1); the solution in liquid Ar at 90 K,  $l = 10\text{ cm}$ ,  $C = 1.5 \cdot 10^{-6}$  mf (4) (b). The  $\nu_1 + \nu_4$  bands of SF<sub>6</sub>; liquid at 222 K,  $l = 0.09\text{ mm}$  (1); the solution in liquid Kr at 174 K,  $l = 2\text{ cm}$ ,  $C = 10^{-4}$  mf (2); the solution in liquid N<sub>2</sub> at 83 K,  $l = 1\text{ cm}$ ,  $C = 10^{-4}$  mf (3) (c). The  $\nu_2 + \nu_4$  bands of CF<sub>4</sub>; the spectrum of liquid at 93 K,  $l = 0.20\text{ mm}$  (1); the solution in liquid Ar at 93 K,  $l = 10\text{ cm}$ ,  $C = 1.5 \cdot 10^{-4}$  mf (4) (d).

0.43 D for SiF<sub>4</sub>. In addition, it can be seen from Figs. 1, *a* and *b* that the center of gravity of the band in liquids (shown by the arrow) shifts only slightly on going to a dilute solution. The bands corresponding to the transitions not including the strong IR-active mode have the Lorentzian profiles in liquid spectra like the bands in dilute solutions, which is evident from Figs. 1, *c* and *d*. Note that the band half-widths are temperature dependent. As an illustration, the  $\nu_2 + \nu_4$  band shapes of pure liquid and dilute solution of CF<sub>4</sub> at the same temperature are displayed in Fig. 1, *d*. One can see that the spectral band widths are in close agreement.

Analogous complex profiles are observed in the spectra of low-temperature liquids of polar molecules. Effect of a permanent dipole moment on the band shape is demonstrated by Fig. 2. One can see that the spectral band shapes of polar liquids, OCS ( $P_0 = 0.72$  D,  $P'_3 = 0.53$  D [34]) and CF<sub>3</sub>Br ( $P_0 = 0.64$  D,  $P'_4 = 0.41$  D), virtually coincide with the band shapes of nonpolar liquids, CO<sub>2</sub> ( $P'_3 = 0.47$  D), BF<sub>3</sub> ( $P'_3 = 0.4$  D [35]).

An additional consequence of Figs. 1 and 2 is the effect of the degeneracy  $g$  of the strong IR active vibration on the manifestation of the resonance dipole–dipole interaction. The considered molecules are characterized by the triply-degenerate (SF<sub>6</sub>, SiF<sub>4</sub>), doubly-degenerate (CF<sub>3</sub>Br, BF<sub>3</sub>) and non-degenerate (OCS, CO<sub>2</sub>) modes. The asymmetry of bands in liquids is seen to be more pronounced on the increase of the mode degeneracy, which is accompanied by the increase of the spectral band widths.

In the following, the main specific features of the band shape formation in the low-temperature liquid spectra caused by the RDD interaction are discussed.

### 3.2 Resonance dipole–dipole interaction

Let us consider a system of two identical molecules whose centers of mass, as well as the point dipoles, are separated by the distance  $R$ . The intramolecular coordinate systems are arbitrarily oriented relatively to the laboratory frame  $X, Y, Z$ . The dipole–dipole interaction energy (in cm<sup>-1</sup>) can be represented as

$$W = \frac{P^{(1)}P^{(2)}}{hcR^3}[(\mathbf{e}^{(1)}\mathbf{e}^{(2)}) - 3(\mathbf{e}^{(1)}\mathbf{e})(\mathbf{e}^{(2)}\mathbf{e})]. \quad (1)$$

Here  $\mathbf{e}^n$  ( $n = 1, 2$ ) are the unit dipole moment vectors for the two molecules in the laboratory frame;  $\mathbf{e}$  is the unit vector connecting the point dipoles;  $P^n$  ( $n = 1, 2$ ) denote the norms of the dipole moment vectors of the molecules, dependent on the vibrational coordinates:

$$P^{(n)} = P_0^{(n)} + P'_k{}^{(n)}q_{k\alpha}^{(n)} \quad (2)$$

where  $P'_k$  is the maximal first derivative of the dipole moment with respect to the normal dimensionless coordinates  $q_k$ ;  $\alpha = x, y, z$ . Other derivatives of the dipole moment are irrelevant to our problem and can be dropped.

The spectrum of a pair of molecules coupled by the RDD interaction can be calculated by using the stationary perturbation theory. The zero-order wave function  $\Phi_L^0 = \Psi_{V_1}^{(1)}\Psi_{V_2}^{(2)}$  is the product of the anharmonic wave functions of two individual molecules, which corresponds to the total energy  $E_L^0 = E_{V_1}^{(1)} + E_{V_2}^{(2)}$  obtained with the anharmonicity taken into account in the second perturbation order.  $V_n$  ( $n = 1, 2$ ) denotes the sets of molecular vibrational quantum numbers. The matrix element  $W$ , dependent on

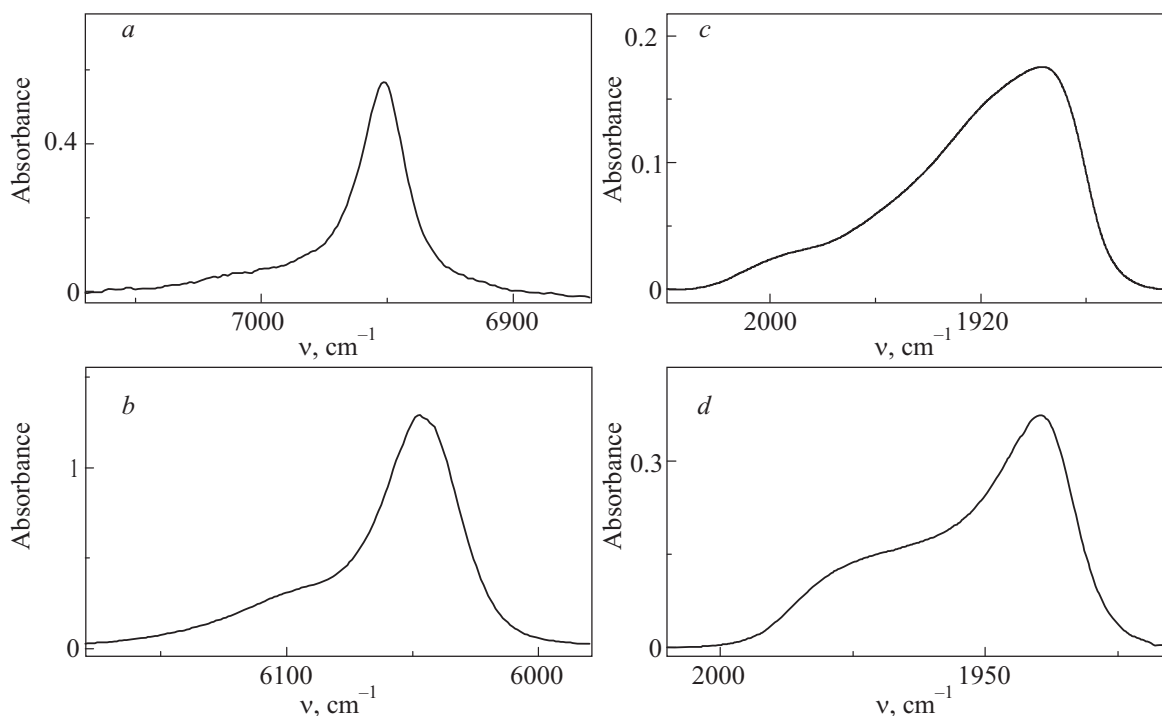


Fig. 2. Infrared spectra of low-temperature polar and nonpolar liquids: the  $3\nu_3$  band of CO<sub>2</sub> (*a*); the  $3\nu_3$  band of OCS (*b*); the  $\nu_3 + \nu_4$  band BF<sub>3</sub> (*c*); the  $\nu_2 + \nu_4$  band of CF<sub>3</sub>Br (*d*).

the mutual orientation of two molecules, can be written as

$$\begin{aligned} W_{LM} &= (hcR^3)^{-1} \langle \nu_i^{(1)} \nu_k^{(1)}; \\ \nu_i^{(2)} \nu_k^{(2)} + 1 | (P_k^1)^2 q_k^{(1)} q_k^{(2)} | \nu_i^{(1)} \nu_k^{(1)} + 1; \\ \nu_i^{(2)} \nu_k^{(2)} \rangle & \Theta^{(12)} = a \Theta^{(12)} \end{aligned} \quad (3)$$

where  $\nu_k$  is the vibrational quantum number of the strong IR-active  $\nu_k$  vibration;  $\nu_i$  is the vibrational quantum number of totally symmetric  $\nu_i$  mode.  $\Theta^{(12)}$  is the orientation-dependent factor whose values lie within the interval  $[-2...2]$ ; the parameter  $a$  is the orientation-independent factor (in  $\text{cm}^{-1}$ )

$$a = P_k^2 / 2hcR^3. \quad (4)$$

The parameter  $a$  has the same value in the region of fundamental and combination modes ( $\nu_i + \nu_k$ ), while in the overtone region  $\nu_k \nu_k$ ,  $a$  is larger by a factor of  $\sqrt{\nu_k}$  [15].

The interaction of two molecules is described by a secular equation whose form depends on the  $\nu_k$  mode degeneracy [33]

$$\begin{vmatrix} E_L^0 - \lambda & W_{LM} \\ W_{LM} & E_M^0 - \lambda \end{vmatrix} = 0. \quad (5)$$

The magnitude of the resonance detuning  $\delta = E_M^0 - E_L^0$  is equal to zero in the fundamental region, and it is governed by the intramolecular anharmonicity in the overtone region. The solution of the secular equation yields the positions of the components of the resonance multiplet and the corresponding corrected eigenfunctions. The intensity of components is proportional to the square of the dipole moment matrix element evaluated with the corrected eigenfunctions. Since the matrix element  $W_{LM}$  depends on  $\Theta^{(12)}$ , the calculated positions of the components also depend on the relative orientation of the interacting molecules. In Ref. 33, analytical expressions for the probability, with which specific values of  $W_{LM}$  occur, have been derived, and the effective Monte Carlo code was developed to simulate the dimer band shapes.

In the case of the interaction of non-degenerate and doubly degenerate oscillators, the continuous spectrum emerges; the dimer band consists of one asymmetric branch in the fundamental region, and of two asymmetric branches, which are separated by a region with zero absorption, in the overtone region.

For the interaction between two triply degenerate oscillators, the mutual orientations of molecules are not essential because the wave functions of isotropic spherical oscillators always can be oriented along the laboratory coordinate axes. The solution of the secular equation leads to the discrete spectrum; the fundamental dimer band has the doublet structure and the overtone dimer band has the quadruplet structure [23,33].

Since the zero-order approximation is the pair of independent molecules with including intramolecular anharmonicity, a nonzero diagonal matrix element  $W_{LL}$  occurs for the polar molecules

$$W_{LL} = (hcR^3)^{-1} \langle 1; 0 | P_0 P_k^{(1)} q_k^{(1)} | 1; 0 \rangle \Theta^{(12)}. \quad (6)$$

The corrections which account for  $W_{LL}$  have no effect on the sharpness of the resonance, because  $W_{LL} = W_{MM}$ , and only a shift of the spectrum as a whole is possible for each arbitrary orientation and the band shape can be only slightly broadened additionally. As an illustration, Fig. 2 shows the band shapes which are equally broadened by the RDD interaction of polar and nonpolar molecular liquids.

To compare these results with experimental data, the calculated profiles must be convolved with a Lorentzian whose half-width is equal to that obtained for an isolated molecule in a liquid solvent.

### 3.3. Dimers as the early stage of cluster formation

Let us consider an application of the above model for the examples of  $(\text{SF}_6)_2$  and  $(\text{OCS})_2$  dimers. Figure 3 demonstrates the experimental and calculated absorption dimer bands of OCS in LKr at 130 K (a) and  $\text{SF}_6$  in LAr at 93 K (b) in the region of the  $\nu_1 + \nu_3$  transition. The shapes were calculated assuming that the RDD interaction encompasses the first coordination sphere. The experimental absorption bands of the dimers have been obtained in the previous studies [23,33] using the follows approaches.

Assuming the concentration of the solute molecules to be low enough, the total concentration  $C$  can be written as

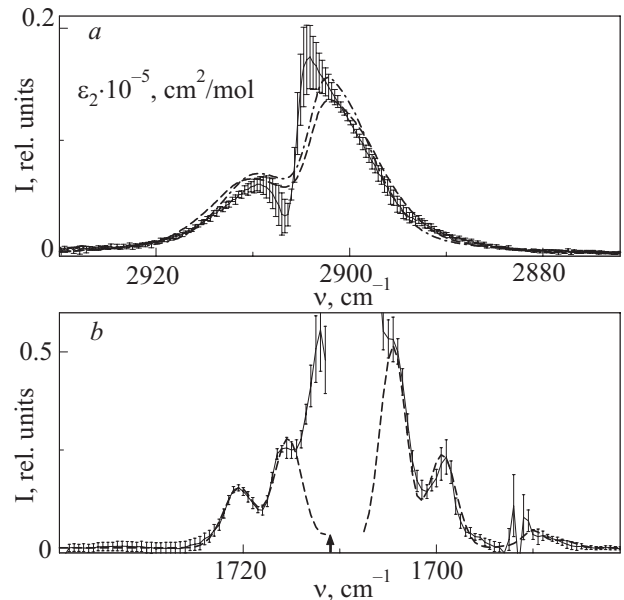


Fig. 3. The spectra of  $(\text{OCS})_2$  (a) and  $(\text{SF}_6)_2$  (b) dimers in the  $\nu_1 + \nu_3$  region in liquid Ar at 93 K. Vertical bars represent the standard deviation at each frequency. The dashed lines represent the calculated spectra. The arrow shows the position of the non-perturbed molecule frequency.

$$C = C_1 + 2C_2 = C_1 + 2kC_1^2 \quad (7)$$

where  $C_1$  and  $C_2$  are concentrations (in mf) of monomers and dimers, respectively, and  $k$  is the monomer–dimer equilibrium constant defined as

$$C_2 = kC_1^2. \quad (8)$$

If  $C_1 \ll 1$  and  $C_2 < C_1$ , then the optical density  $D = \lg(I_0/I)$  at frequency  $\nu$ , reduced to unit optical path length, can be described by

$$D(\nu) = \varepsilon_1(\nu)C_1 + \varepsilon_2(\nu)C_2 = \varepsilon_1C + k(\varepsilon_2 - 2\varepsilon_1)C^2 \quad (9)$$

where  $\varepsilon_1$  and  $\varepsilon_2$  are, respectively, the absorption coefficient of monomer and dimers at a frequency  $\nu$ . For a given concentration  $C_i$ , expression (9) can be rewritten in the form

$$D_i(\nu) = D/C_i = \varepsilon_1(\nu) + \Delta\varepsilon(\nu)C_i \quad (10)$$

where  $\Delta\varepsilon(\nu) = k(\varepsilon_2 - 2\varepsilon_1)$ . Solution of the abundant system of equations by the least squares method for the whole set of spectra at different concentrations gives the absorption coefficients  $\varepsilon_1$  and  $\Delta\varepsilon$ . To determine the absorption coefficient  $\varepsilon_2(\nu)$  of a dimer, the constant  $k$  must be known. In Ref. 36, the constant  $k$  was estimated to be  $k = 6 \text{ mf}^{-1}$  based on entirely statistical treatment of the distribution of molecules in liquid.

Returning to Fig. 3, one can see that the continuous spectrum of the OCS dimer consists of two asymmetric broad branches while the  $\text{SF}_6$  dimer spectrum has a more narrow structure. The band shape of OCS dimer was calculated with the value of the anharmonicity detuning  $\delta = x_{13} = -3.4 \text{ cm}^{-1}$  [34] and different values of the fitting parameter  $a$  varying from 6 to 7  $\text{cm}^{-1}$  (dashed and dash dotted lines). The optimal agreement between the simulated and experimental profiles is achieved with  $a = 7 \text{ cm}^{-1}$  that gives  $R = 4.75 \text{ \AA}$ .

For  $\text{SF}_6$  dimer the optimal band shape (dashed line) is obtained with  $a = 5.1(1) \text{ cm}^{-1}$ ,  $R = 5.22 \text{ \AA}$ , and  $\delta = x_{13} = -3 \text{ cm}^{-1}$ . An additional fifth component located at the frequency of the anharmonic detuning  $\delta$  (indicated by arrow) belongs to the absorption of the dimer with the doubled distance  $R_{SS}$ . The absorption in the spectral region of  $1690 \text{ cm}^{-1}$  pertains to the band of the monomer  $^{34}\text{SF}_6$ . Within the limit of experimental uncertainties [23], the  $(^{34}\text{SF}_6)_2$  dimer spectrum can be described by the same value of the parameter  $a$ .

In the fundamental region, for which the resonance detuning is equal to zero, the dimer bands strongly overlap with the monomer ones, which appreciably hinders the determination of the dimer absorption coefficient  $\varepsilon_2(\nu)$ . For this reason, the fundamental dimer bands are best observed in spectra with relative narrow bands of a monomer. Thus, in cryosolution, the absorption of dimer can be obtained only for  $\text{SF}_6$  molecule owing to the small contributions of other broadening mechanisms. The half-width of the monomer band is about  $1 \text{ cm}^{-1}$  [23].

Figure 4 exhibits the absorption spectra of  $\text{SF}_6$  solution in liquid  $\text{N}_2$  at 83 K in the region of the  $\nu_3$  transition. The fraction of the absorption proportional to the square of the solute concentration, i.e., the absorption of the dimer ( $b$ ) was isolated as the difference between the experimental spectra shown in Fig. 4, *a*. One can see that the dimer band is a doublet splitted by  $\Delta\nu = 16.2 \text{ cm}^{-1}$ . The value of the parameter  $a$  is found to be  $a = 5.4 \text{ cm}^{-1}$  from which  $R = 5.2 \text{ \AA}$  follows, in a good agreement with the result obtained from the combination band data.

One of the most informative methods to study the fundamental dimer bands is the method of the infrared matrix isolation spectroscopy. When dimers are trapped in low-temperature matrices, the interacting molecules have well-defined orientations and the bands are much narrower than in liquids. Thanks to this fact it is possible to determine the symmetry of a dimer and the distance between centers of mass of two interacting molecules. To illustrate the general situation, the absorption of  $(\text{SF}_6)_2$  and  $(\text{SiF}_4)_2$  dimers in Ar matrices are displayed on Figs. 5 and 6, respectively.

Figure 5 presents the  $\nu_3$  region in spectra of  $\text{SF}_6/\text{Ar}$  matrices with natural abundance of sulfur isotopes at concentrations differing by an order of magnitude (*a*) and the ab-

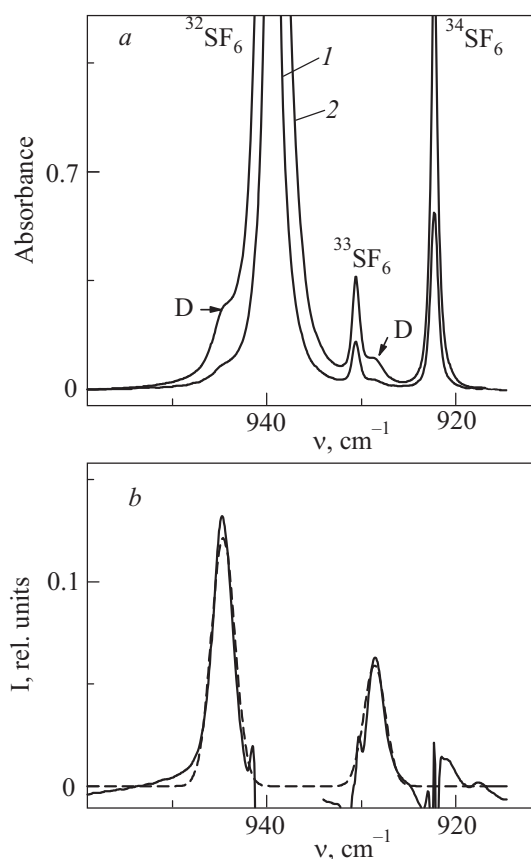


Fig. 4. The  $\nu_3$  region in the spectrum of  $\text{SF}_6$  solution in liquid  $\text{N}_2$  at 83 K: experimental spectra at  $1 \cdot 10^{-2} \text{ mol/l}$  (1) and  $2.5 \cdot 10^{-2} \text{ mol/l}$  (2) with  $l = 0.04 \text{ cm}$  (*a*); the dimer  $(\text{SF}_6)_2$  spectrum, dashed line represents the calculated spectrum (*b*). The bands labeled by  $^{32}\text{SF}_6$ ,  $^{33}\text{SF}_6$ ,  $^{34}\text{SF}_6$  are the monomers bands of isotopomers. The dimer bands are marked by D.

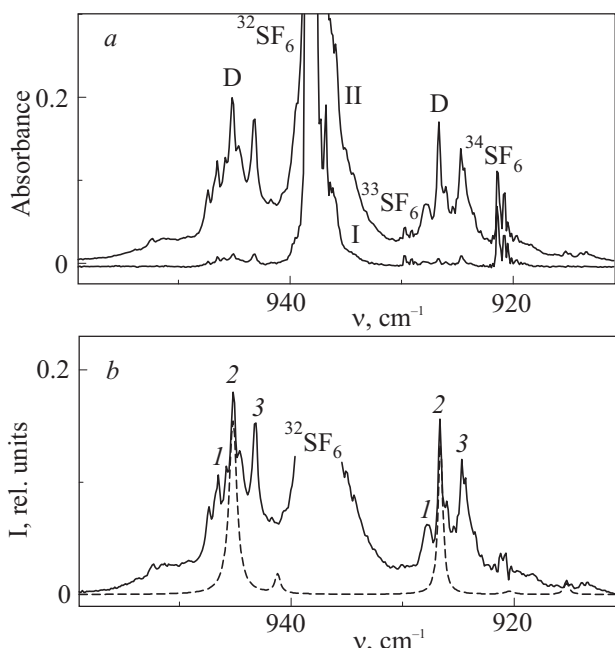


Fig. 5. The  $\nu_3$  region in the spectra of SF<sub>6</sub>/Ar matrices at 11 K: experimental spectra of concentrations 1/16000 (I) and 1/2000 (II) (a); the spectrum of (SF<sub>6</sub>)<sub>2</sub> dimer (solid line), and the calculated dimer bands for one of sites (dashed line) (b). The site components are marked by 1, 2, and 3. The bands labeled by <sup>32</sup>SF<sub>6</sub>, <sup>33</sup>SF<sub>6</sub>, <sup>34</sup>SF<sub>6</sub> are the monomers bands of isotopomers. The dimer bands are marked by D.

sorption dimer band (b) obtained as the difference between these spectra. The band of the isotopically substituted <sup>34</sup>SF<sub>6</sub> molecule was used to control the procedure for separating out the absorption quadratic in concentration. It can be seen from Fig. 5 that the dimer band has the characteristic site structure indicated by 1, 2, 3. The resonance splitting  $\Delta\nu$  for all three sites has the same value within experimental error and is equal to 18.45(5) cm<sup>-1</sup>, which gives  $a = 6.15$  cm<sup>-1</sup>. The dashed line shows the dimer spectrum calculated for the most intense site 2 by taking into account the RDD and dipole-induced dipole (DID) interactions. The individual component was fitted by a Lorentzian with a width of about 0.6 cm<sup>-1</sup>. The calculation is seen to be in semiquantitative agreement with the experimental data. Additional allowance for the DID interaction leads to a refinement of the value of the parameter  $a = 5.9(1)$  cm<sup>-1</sup>, from which one can find the value of  $R = 5.1$  Å. The obtained symmetry of the dimer in Ar matrix is  $D_{2d}$  that responds well to the result of Ref. 32.

The (SiF<sub>4</sub>)<sub>2</sub> dimer in the Ar matrix is characterized by two bands without site structure, as is evident in Fig. 6, b. The splitting value  $\Delta\nu = 24.2$  cm<sup>-1</sup> and the derived value of the distance  $R = 4$  Å. The spectral data on the SiF<sub>4</sub>/Ar matrices from Ref. 28 show the SiF<sub>4</sub> dimer to have the  $D_{2d}$  symmetry that is different from the result of Ref. 31. The ab initio calculations show that the dimer symmetry varies from  $C_s$  to  $C_{2h}$  [28].

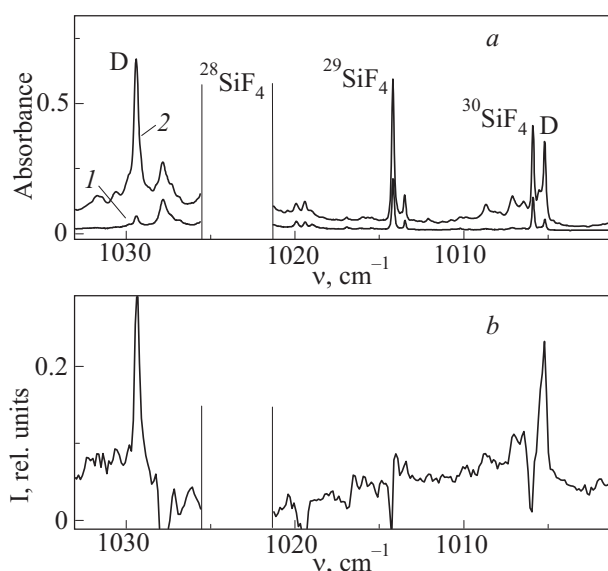


Fig. 6. The  $\nu_3$  region in the spectra of SiF<sub>4</sub>/Ar matrices at 11 K: experimental spectra of concentrations 1/10000 (I) and 1/1000 (2) (a); the spectrum of (SiF<sub>4</sub>)<sub>2</sub> dimer (b). The bands labeled by <sup>28</sup>SiF<sub>4</sub>, <sup>29</sup>SiF<sub>4</sub>, <sup>30</sup>SiF<sub>4</sub> are the monomers bands of isotopomers. The dimer bands are marked by D.

Table 1 summarizes the data on the minimal distance  $R_{nm}$  between two interacting molecules obtained for different low-temperature molecular systems. For each system reasonable values of  $R_{nm}$  are found, which are close to the values derived from the density of liquid  $\rho$  via  $R = (\sqrt{2} / \rho_{\text{melt}})^{-1/3}$ .

Table 1. Values of the minimal distance  $R_{nm}$  between nearest interacting molecules obtained by different studies of low-temperature molecular systems

| Mole-<br>cule    | $P'_3$ ,<br>D | $T_{\text{melt}}$ ,<br>K | R, Å |              |                                 |                      |      |
|------------------|---------------|--------------------------|------|--------------|---------------------------------|----------------------|------|
|                  |               |                          | 1    | 2            | 3                               | 4                    | 5    |
| SF <sub>6</sub>  | 0.55          | 222                      | 5.71 | 5.47         | 5.1(Ar)<br>5.9(N <sub>2</sub> ) | 5.2(Ar)              | 4.75 |
| SiF <sub>4</sub> | 0.43          | 186                      | 5.32 | 5.3          | 4.0(Ar)                         | 4.8(Ar)              | 4.19 |
| CF <sub>4</sub>  | 0.465         | 89                       | 4.78 | 4.63<br>4.40 | 4.18(Ar)<br>4.03(Ne)            | 4.85(Ar)             |      |
| NF <sub>3</sub>  | 0.42          | 66                       | 4.46 | 4.4          |                                 | 4.5(Ar)              |      |
| OCS              | 0.53          | 134                      | 4.75 | 4.7          |                                 | 4.7(O <sub>2</sub> ) |      |

Notes: 1 — Data found from the liquid density, 2 — spectra of liquid at temperature close to the melting point, 3 — dimers spectra in Ar, N<sub>2</sub> (11 K), and Ne (4.7 K) matrices, 4 — solutions in liquid Ar, O<sub>2</sub> (93 K) and Kr (130 K), 5 — molecular beam experiments (1–3 K) [31,32].

Let us consider the changes in the spectrum when one molecule comes into the first coordination sphere of the other. As an example, scrutinize the interaction between OCS molecules for which the interaction matrix element  $W_{LM}$  has the minimal value. Figure 7 displays the shapes of  $\nu_3$ ,  $2\nu_2 + \nu_3$ , and  $2\nu_3$  bands of (OCS)<sub>2</sub> dimer in liquid

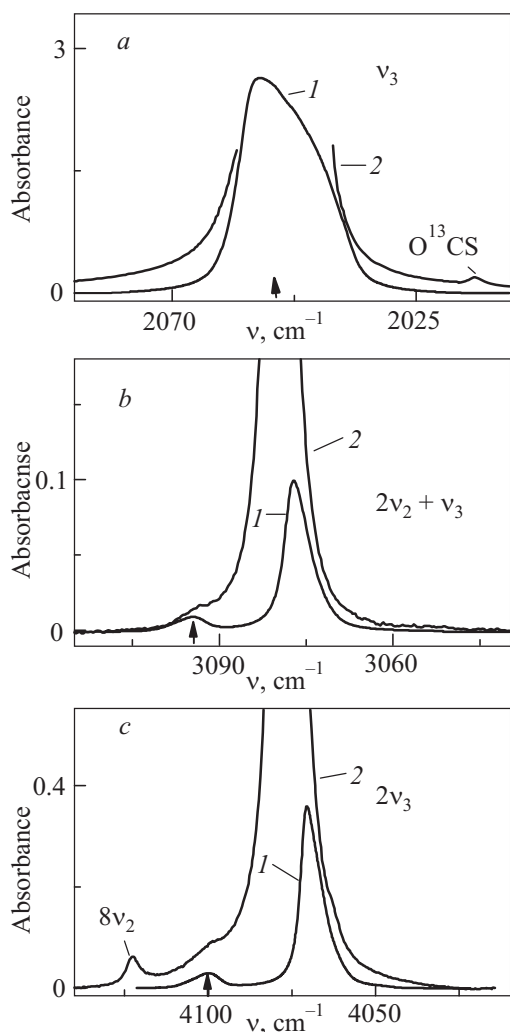


Fig. 7. The calculated (1) and experimental (2) spectra of  $v_3$  (a),  $2v_2 + v_3$  (b), and  $2v_3$  (c) bands of  $(\text{OCS})_2$  dimer in liquid Kr at 130 K. The arrow shows the position of the frequency of the non-perturbation molecule.

Kr at 130 K together with experimental spectra at the concentration  $C = 0.01$  mf. The profiles were calculated in a crude approximation with the values of  $R_m = 4.75 \text{ \AA}$  found from the liquid density, the dipole moment first derivative  $P'_3 = 0.53 \text{ D}$  obtained in Ref. 34, and the dimerization constant  $k = 6 \text{ mf}^{-1}$  estimated in Ref. 36. Note that for  $C = 0.01 \text{ mf}$  and  $k = 6 \text{ mf}^{-1}$ , it follows from Eq. (8) that the concentration of dimerized molecules is about 10%. As is evident from Fig. 7,a, the entire fundamental dimer band falls within the region of unreliability. In the region of the  $2v_2 + v_3$  and  $2v_3$  transition, new components appear in the spectra in the high-frequency wing, shifted from the main maximum by the value of the corresponding anharmonicity detuning  $\delta$  (indicated by the arrow), as can be seen in Figs. 7,b and c. The value of  $\delta = 2x_{23} = -24 \text{ cm}^{-1}$  in the  $2v_2 + v_3$  region, and  $\delta = 2x_{33} = -14 \text{ cm}^{-1}$  in the  $2v_3$  region. These additional components can be assigned with confidence to OCS dimers. The formation of dimers is more pronounced

in the spectra for a larger value of the anharmonicity constant that governs the resonance detuning.

## 6. Clusters

Let us consider the low-temperature molecular liquids ( $\text{CF}_4$ ,  $\text{NF}_3$ , and  $\text{OCS}$ ) with large concentrations ( $C > 0.1 \text{ mf}$ ) when the coordination sphere contains one or more dissolved molecules. Figure 8 displays the absorption spectra of  $\text{NF}_3$  dissolved in  $\text{LO}_2$  at 90 K in the  $v_1 + v_3$  region at the concentration varying from 0.3 mf to pure liquid. The behavior of band shapes is conveniently described with the use of the spectral moments [37]

$$M(m) = M(0)^{-1} \int I(\nu) [\nu - M(1)]^m d\nu \quad (11)$$

where  $m = 2, 3, \dots$ ,  $M(0) = \int I(\nu) d\nu$  is the integrated intensity, and  $M(1) = M(0)^{-1} \int \nu I(\nu) d\nu$  is the center of gravity of the band. As can be seen from Fig. 8,  $M(0)$  and  $M(1)$  remain unchanged within the experimental error on going from the spectrum of solution to the pure liquid spectrum, while the second spectral moment  $M(2)$ , which defines the band width, and the third spectral moment  $M(3)$  describing the band asymmetry considerably increase with concentration.

In Ref. 15 the general expression for the  $m$ th spectral band moment has been derived to be  $M(m) = (W^m)_{00}$  (see Appendix 1 in Ref. 15), which allows one to explain some experimental data without solving the secular equation. Consider the RDD interaction of a particular molecule (denoted by index 0) with  $n$  molecules of the first coordination sphere with the radius  $R$ . After averaging over possible molecular orientations (see Appendix 2 in Ref. 15), the

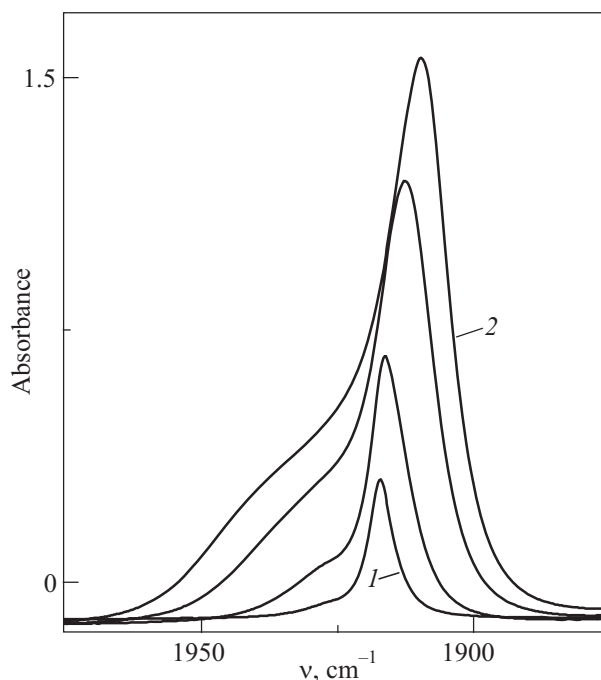


Fig. 8. Concentration dependence of the  $v_1 + v_3$  band of  $\text{NF}_3$  dissolved in liquid oxygen at 90 K. The  $\text{NF}_3$  concentration varies from 0.3 (curve 1) to 1 (curve 2) mf.

analytical expressions for the second and third spectral moments,  $M(2)$  and  $M(3)$ , can be given as

$$M(2) = \sum_{k=1}^n (W_{0k})^2 = 2a^2 g n_2 / 3, \quad (12)$$

$$M(3) = \sum_{k,i=1}^n (W_{ok} W_{ki} W_{i0}) = 11a^3 g^2 n_3 / 36 + \delta M(2) \quad (13)$$

where  $a$  is given by Eq. (4),  $g$  denotes the degeneracy of oscillators,  $\delta$  is the anharmonic detuning,  $n_2$  is the number of pairs of interacting molecules separated by the distance  $R$ , which includes the central molecule, and  $n_3$  is the number of groups of three interacting molecules, each group contains the central one and two molecules from the first coordination sphere.

The behavior of  $M(2)$  and  $M(3)$  spectral moments as functions of concentration for  $\nu_1 + \nu_3$  bands of  $\text{CF}_4$  solution in LAr [37] and  $\text{NF}_3$  solution in  $\text{LO}_2$ , and for  $2\nu_2 + \nu_3$

band of  $\text{OCS}$  solution in LKr [34] are displayed in Fig. 9. Values of  $M(2)$  and  $M(3)$  are determined only by the RDD interaction, and are obtained by subtracting the corresponding values for a highly diluted solution ( $C < 10^{-4}$  mf) from the experimental data. As evident from Fig. 9,  $M(2)$  linearly increases with increasing concentration (plots on the left-hand side), while  $M(3)$  increases with concentration in a nonlinear manner (plots on the right-hand side). Thus, in complete accordance with Eqs. (12) and (13), the second and third spectral moments are determined by the number of pair and triple interactions with molecules within the first coordination sphere, respectively.

The parameter  $n_3$  can be correlated with the parameter  $n_2$  via

$$n_3 = 2/[11n_2(n_2-1)] \quad (14)$$

by assuming that the first coordination sphere represents a well ordered closely packed structure with the coordination

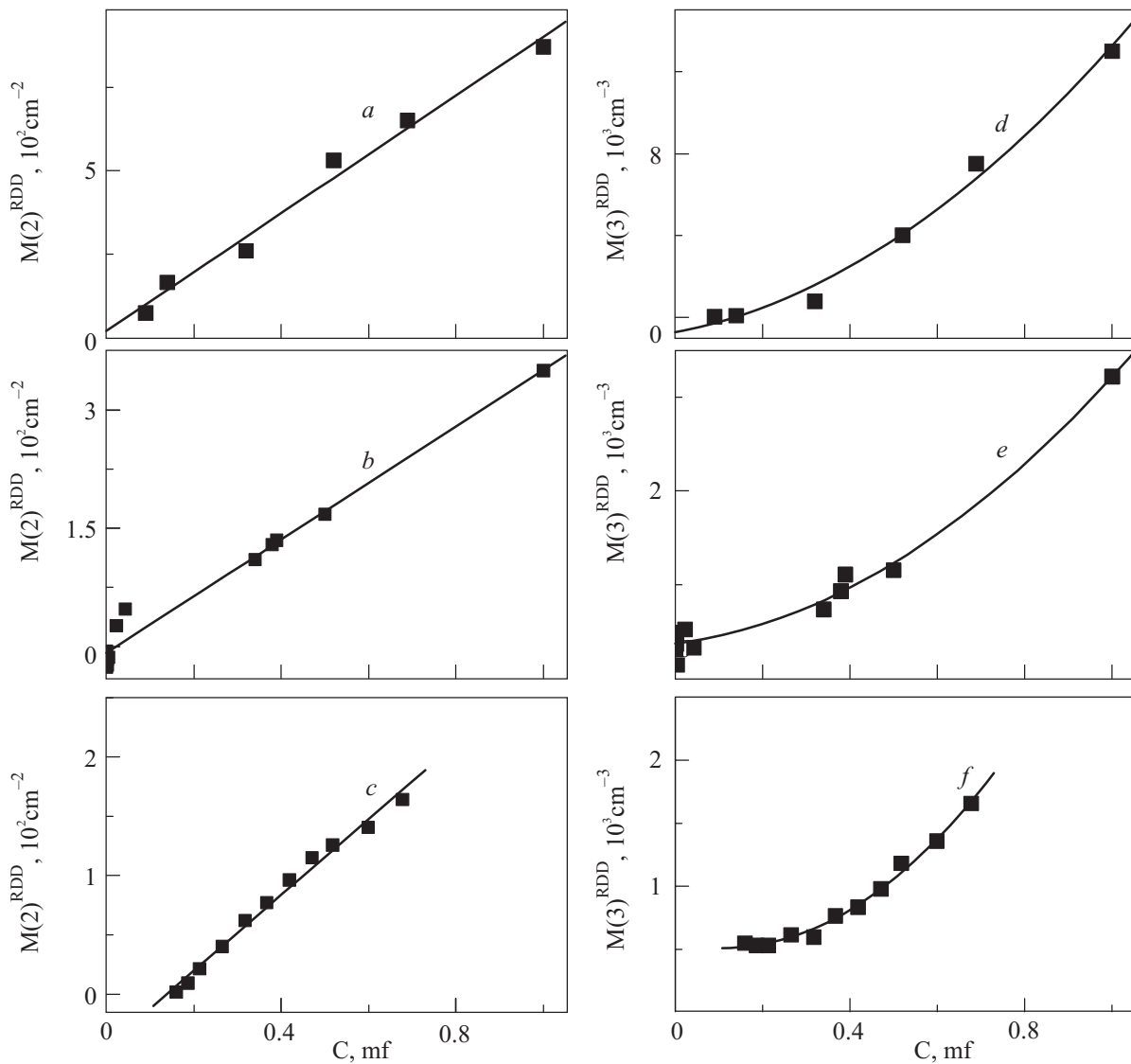


Fig. 9. Concentration dependence of the  $M(2)^{RDD}$  (a, b, c) and  $M(3)^{RDD}$  (d, e, f) in the  $\nu_1 + \nu_3$  region of  $\text{CF}_4$  solution in liquid Ar (a, d), the  $\nu_1 + \nu_3$  region of  $\text{NF}_3$  solution in liquid  $\text{O}_2$  (b, e), and the  $2\nu_2 + \nu_3$  region of  $\text{OCS}$  solution in liquid Kr (c, f).

number  $n$  equals to 12. The size of the solvent molecule is taken to be close to that of the solute molecule, and the interaction energy between solvent molecules and between solvent and solute molecules equals that of solute molecules with themselves. The spatial distribution of solute molecules in the solvent quasi-lattice is taken to be random. The dependence of the parameter  $n_3$  on  $n_2$  calculated in this approximation is shown in Fig. 10 by the solid line.

Note that there exists some ambiguity in the parameter  $a$  for the studied liquid. For example,  $a = 5.5 \text{ cm}^{-1}$  for liquid  $\text{CF}_4$  at temperature close to the melting point [18] and  $a = 7.0 \text{ cm}^{-1}$  found from the density of liquid at the same temperature. Figure 10,*a* displays the calculated correlation of  $n_3$  and  $n_2$  parameters by using the experimental data on the  $M(2)$  and  $M(3)$  spectral moments for solution of  $\text{CF}_4$  in LAr with  $a$  varying from 5.5 to 7.1  $\text{cm}^{-1}$ . One can see that the weak dependence on the value of the parameter  $a$  is observed.

The dependences of  $n_3$  on  $n_2$  calculated from Eqs. (12) and (13) with the experimental values of the spectral band moments for  $\text{CF}_4$  solution in LAr,  $\text{NF}_3$  solution in  $\text{LO}_2$ ,

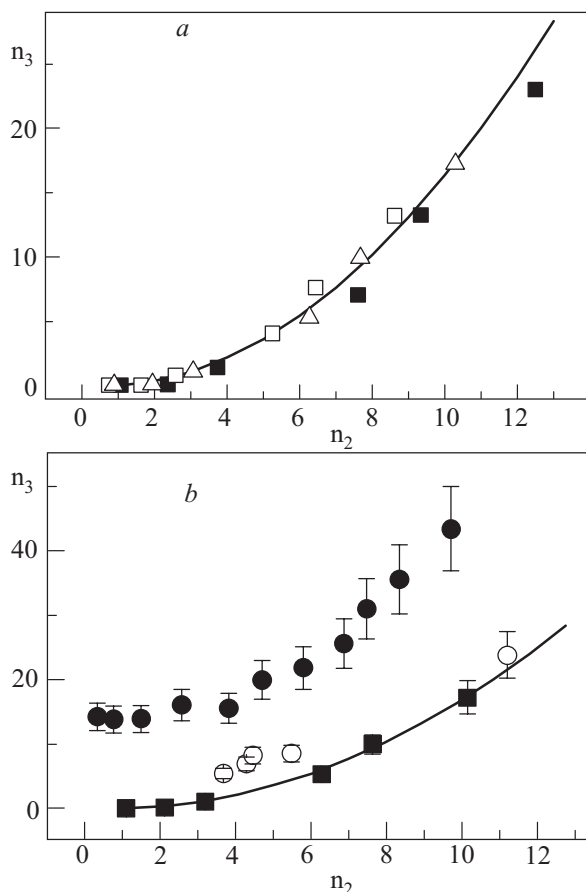


Fig. 10. Calculated correlation between the parameters  $n_3$  and  $n_2$ . The solution of  $\text{CF}_4$  in liquid Ar at 93 K, with  $a = 5.5$  (■), 6.5 (□), and 7.1 ( $\Delta$ )  $\text{cm}^{-1}$  (*a*); the solutions: of  $\text{CF}_4$  ( $a = 6.5 \text{ cm}^{-1}$ ) in liquid Ar (■), of  $\text{NF}_3$  ( $a = 4.8 \text{ cm}^{-1}$ ) in liquid  $\text{O}_2$  (○), of  $\text{OCS}$  ( $a = 5.0 \text{ cm}^{-1}$ ) in liquid Kr (●) (*b*). Solid line represents the dependence calculated by Eq. (15).

and  $\text{OCS}$  solution in LKr are depicted in Fig. 10,*b*. Few conclusions can be drawn from this figure. First, the calculated correlation of  $n_3$  and  $n_2$  parameters by using the experimental data for  $\text{CF}_4$  solution is in accordance with the suggested model. Second, for the  $\text{NF}_3$  molecule, the discrepancy between the predicted and experimental behavior of  $n_3$  vs  $n_2$  is observed in the concentration range  $C = (0.2\text{--}0.5)$  mf. It can be assumed that compact aggregates arise primarily in this case, the solute molecules approach closely one another. Unlike the carbon tetrafluoride,  $\text{NF}_3$  is not spherical molecule possessing the small permanent dipole moment  $P_0 = 0.2 \text{ D}$ . Third, for the  $\text{OCS}$  molecule, a large deviation between the predicted and experimental behavior of  $n_3$  vs  $n_2$  is also observed, which probably is due to the fact that even at small concentrations the solute molecules tend to aggregate [9].  $\text{OCS}$  is a linear polar molecule ( $P_0 = 0.8 \text{ D}$ ), the coordination number  $n_2$  in pure liquid varies from 14 to 17 [38].

## 7. Conclusions

The main specific features of manifestations of the RDD interaction in the spectra of low-temperature systems consisting of the molecules with the large first derivatives (more than 0.3 D) of the dipole moment are studied. The calculations using the RDD interaction model are in good agreement with the experimental data on the spectra of low-temperature matrices ( $\text{CF}_4/\text{Ar}$  (Ne),  $\text{SF}_6/\text{Ar}$  (Xe,  $\text{N}_2$ ), and  $\text{SiF}_4/\text{Ar}$  (Xe,  $\text{N}_2$ ) at 4,7 (11) K), of low-temperature liquids ( $\text{CF}_4$  at 90–130 K,  $\text{SF}_6$  at 222 K,  $\text{NF}_3$  at 90 K,  $\text{OCS}$  at 135 K,  $\text{CO}_2$ ,  $\text{CF}_3\text{Br}$ ,  $\text{CF}_3\text{Cl}$ , and  $\text{BF}_3$ ), and of their solutions in cryosolvents (Ar at 90–130 K,  $\text{O}_2$  at 90–130 K,  $\text{N}_2$  at 77–130 K, Kr at 143 K, and Xe at 175 K). The RDD interaction is shown to manifest itself not only in the fundamental bands which are intense in the IR absorption, but also in the overtone and combination bands which include the strongly IR-active fundamental. The presence of the permanent dipole moment has no effect on the sharpness of the resonance.

The use of the manifestations of the RDD interaction found in the spectrum of a pair of molecules allows us to detect the entry of the light-absorbing molecule into the first coordination sphere. The sensitivity of this method is increased for the spectra in the overtone region.

Based on the stationary perturbation theory and taking into account for the intermolecular resonance, the rough model was developed to detect pairs of interacting molecules and clusters in the low-temperature molecular systems. The study of experimental values of second- and third-order spectral moments allows one to estimate the number of molecules in a cluster.

Generally, our results demonstrate the high potential of the IR spectroscopy as a tool to study the dimer and cluster formation in the low-temperature molecular systems.

1. *Molecular Cryospectroscopy*, R.J.H. Clark and R.E. Hester, (eds.) Wiley, New York (1995), v. 23.
2. G. Strauss, H. Zweier, H. Bertagnolli, T. Bausenwein, K. Todheide, and P. Chieux, *J. Chem. Phys.* **101**, 662 (1994).
3. A.P. Isakina, A.I. Prokhvatilov, and J. Rodriguez-Carvajal, *Fiz. Nizk. Temp.* **26**, 404 (2000) [*Low Temp. Phys.* **26**, 296 (2000)].
4. G. Finarescu, D. Luckhaus, and R. Signorell, *J. Chem. Phys.* **128**, 184301 (2008).
5. M.A. Ovchinnikov and C.A. Wight, *J. Chem. Phys.* **99**, 3374 (1993).
6. S. Nose and M.L. Klein, *J. Chem. Phys.* **78**, 6928 (1983).
7. C.G. Gray and K.E. Gubbins, *Theory of Molecular Fluids Fundamentals, Int. Ser. Monogr. Chem.*, Oxford Science, Oxford (1984), v. 9.
8. A.I. Burshtein and S.I. Temkin, *Spectroscopy of Molecular Rotation in Gases and Liquids*, Cambridge University Press, Cambridge (1994).
9. D. Dellis and J. Samios, *Chem. Phys.* **192**, 281 (1995).
10. L. Chen, R. Zheng, Q. Sci, and Y.J. Yan, *J. Chem. Phys.* **131**, 094502 (2009).
11. M. Yvinec and R.M. Pick, *J. Chem. Phys.* **71**, 3440 (1979).
12. M. Gilbert and M. Drifford, *J. Chem. Phys.* **65**, 923 (1976); *ibid.* **66**, 3205 (1977).
13. M. Gilbert, P. Nectoux, and M. Drifford, *J. Chem. Phys.* **68**, 679 (1978).
14. A. Vinit, J. Lambard, P. Nectoux, and M. Gilbert, *Chem. Phys. Lett.* **63**, 460 (1979).
15. T.D. Kolomiitsova, A.P. Burtsev, V.G. Fedoseev, and D.N. Shchepkin, *Chem. Phys.* **238**, 315 (1998).
16. A.P. Burtsev, T.D. Kolomiitsova, and D.N. Shchepkin, *Chem. Phys. Lett.* **379**, 495 (2003).
17. V.N. Bocharov, A.P. Burtsev, T.D. Kolomiitsova, and D.N. Shchepkin, *Opt. Spectrosc.* **100**, 382 (2006).
18. D.S. Andrianov, A.N. Cherevatova, T.D. Kolomiitsova, and D.N. Shchepkin, *Chem. Phys.* **364**, 69 (2009).
19. N.N. Filippov, *Khim. Fiz.* **11**, 1157 (1992).
20. V.A. Kondaurov, S.M. Melikova, and D.N. Shchepkin, *Opt. Spectrosc.* **56**, 626 (1984).
21. J. Geraedts, S. Setiadi, S. Stolte, and J. Reuss, *Chem. Phys. Lett.* **78**, 277 (1981).
22. M. Snels and J. Reuss, *Chem. Phys. Lett.* **140**, 543 (1987).
23. T.D. Kolomiitsova, A.P. Burtsev, O.G. Peganov, and D.N. Shchepkin, *Opt. Spectrosc.* **84**, 381 (1998).
24. T.D. Kolomiitsova, V.A. Kondaurov, and D.N. Shchepkin, *Opt. Spectrosc.* **91**, 203 (2001).
25. T.D. Kolomiitsova, D.N. Shchepkin, K.G. Tokhadze, W.A. Herrebout, and B.J. van der Veken, *J. Chem. Phys.* **121**, 1504 (2004).
26. T.D. Kolomiitsova, Z. Mielke, D.N. Shchepkin, and K.G. Tokhadze, *Chem. Phys. Lett.* **357**, 181 (2002).
27. A.N. Cherevatova, T.D. Kolomiitsova, D.N. Shchepkin, K.G. Tokhadze, Z. Mielke, S. Coussan, and P. Roubin, *J. Mol. Spectrosc.* **238**, 64 (2006).
28. S.K. Ignatov, T.D. Kolomiitsova, Z. Mielke, A.G. Razuvaev, D.N. Shchepkin, and K.G. Tokhadze, *Chem. Phys.* **324**, 753 (2006).
29. I.K. Tokhadze, T.D. Kolomiitsova, K.G. Tokhadze, and D.N. Shchepkin, *Opt. Spectrosc.* **102**, 446 (2007).
30. A.D. Afanasiev, A.A. Ivanov, F. Luty, et al., *Radiat. Eff. Defects Solids* **151**, 311 (1999).
31. R.-D. Urban and M. Takami, *J. Chem. Phys.* **102**, 3017 (1995).
32. R.-D. Urban and M. Takami, *J. Chem. Phys.* **103**, 9132 (1995).
33. D.S. Andrianov, A.S. Blagoveshchenskii, T.D. Kolomiitsova, and D.N. Shchepkin, *Opt. Spectrosc.* **94**, 513 (2003).
34. V.N. Bocharov, A.P. Burtsev, O.S. Gulidova, T.D. Kolomiitsova, and D.N. Shchepkin, *Opt. Spectrosc.* **105**, 242 (2008).
35. W. Vanspeybroec, *Author's Abstract of Doctoral Dissertation*, Antwerp (2006).
36. A.N. Cherevatova, D.N. Shchepkin, and W. Herrebout, *Abstracts of Reports XVth Symposium on High Resolution Molecular Spectroscopy*, Tomsk (2009), p. 45.
37. T.D. Kolomiitsova, V.G. Fedoseev, and D.N. Shchepkin, *Opt. Spectrosc.* **79**, 523 (1995).
38. J. Samios, H. Stassen, and T. Dorfmueller, *Chem. Phys.* **160**, 33 (1992).